

Observation of Microscopic Diffusion Anisotropy in the Spinal Cord Using Double-Pulsed Gradient Spin Echo MRI

M.E. Komlosh,^{1*} M.J. Lizak,² F. Horkay,¹ R.Z. Freidlin,³ and P.J. Basser¹

A double-pulsed gradient spin echo (d-PGSE) filtered MRI sequence is proposed to detect microscopic diffusion anisotropy in heterogeneous specimen. The technique was developed, in particular, to characterize local microscopic anisotropy in specimens that are macroscopically isotropic, such as gray matter. In such samples, diffusion tensor MRI (DTI) produces an isotropic or nearly isotropic diffusion tensor despite the fact that the medium may be anisotropic at a microscopic length scale. Using d-PGSE filtered MRI, microscopic anisotropy was observed in a “gray matter” phantom consisting of randomly oriented tubes filled with water, as well as in fixed pig spinal cord, within a range of b-values that can be readily achieved on clinical and small animal MR scanners. These findings suggest a potential use for this new contrast mechanism in clinical studies and biological research applications. Magn Reson Med 59:803–809, 2008. © 2008 Wiley-Liss, Inc.

Key words: MRI; double; pulsed gradient; diffusion; anisotropy; multiple scattering; white matter; gray matter; spinal cord; phantom; filter; DTI

Diffusion tensor imaging (DTI) is a powerful tool for characterizing normal and abnormal brain development as well as pathological changes and aging (1). It can readily detect anisotropic diffusion in white matter comprised of long coherent axons (Fig. 1d), whose extent usually exceeds the MRI voxel length scale (Fig. 1e). By acquiring diffusion-weighted imaging (DWI) data (2,3) with a multiplicity of gradient directions, an apparent diffusion tensor can be estimated, from which one can characterize the degree of voxel-averaged diffusion anisotropy (1) (Fig. 1f). However, difficulties in DTI anisotropy measurements arise when the material's local directors show a large spread of orientations on the voxel length scale. Such is the case for gray matter, which consists of multiple cell types and axonal and dendritic fibers (Fig. 1a) that may be individually anisotropic, but are randomly oriented on a voxel length scale (Fig. 1b). As a result, its apparent diffu-

sion tensor appears considerably less anisotropic than that of the white matter (4–7) (Fig. 1c).

Unlike the single-pulsed gradient spin echo (PGSE) experiment (8), multiple PGSE experiments (9–11) can detect microscopic anisotropy in materials that are macroscopically isotropic. These techniques extend the Stejskal-Tanner PGSE sequence, which uses a single pair of diffusion gradient pulses, to sequences having multiple pairs of gradient pulses. In practice, all current multiple PGSE methods use only two blocks of PGSE gradient pulse pairs, where in most only two sets of experiments are performed. In the first experiment the gradients are applied along the same direction (i.e., are collinear) and in the second gradients are perpendicular to each other (i.e., are orthogonal). For a PGSE experiment on an anisotropic sample, such as an impermeable tube for example, the echo attenuation resulting from diffusion along the tube axis will differ from the diffusion perpendicular to the tube axis. However, when those tubes are randomly oriented, the PGSE echo attenuations will become independent of the gradient pulse direction. The echo attenuation resulting from two sequential PGSE blocks is essentially a multiplication of the mean square displacement signal resulting from each PGSE block, which is then integrated over the entire sample. Thus, for randomly oriented tubes the echo attenuation will depend on whether the two PGSE blocks were collinear or orthogonal. In such a medium the echo attenuation will be greater when the PGSE blocks are orthogonal than when they are collinear. A difference between the collinear and orthogonal double (d)-PGSE experiments reveals microscopic anisotropy in the sample. Note that for an isotropic sample the resulting echo attenuation is independent of the direction of the applied gradient pulses in the PGSE blocks; thus, in both sets of experiments the d-PGSE will be identical. One- and two-dimensional d-PGSE NMR spectroscopy sequences (12,13) have been used to characterize local anisotropy of macroscopically isotropic materials, such as liquid crystals (11), prolate yeast cells (10), plants (14), and, recently, gray matter (15).

These d-PGSE NMR techniques, however, are not adequate to characterize inhomogeneous specimen (e.g., consisting of multiple regions each with a unique microarchitecture) or in vivo samples, for which a d-PGSE MRI sequence should be used. The ability to measure microscopic anisotropy in vivo in gray matter (and other complex tissue types) could lead to a new source of MR contrast capable of discriminating between subtle microarchitectural and microstructural tissue characteristics that cannot currently be detected using DTI. d-PGSE MRI imaging was first used by Koch and Finsterbusch (16), but for

¹Section on Tissue Biophysics and Biomimetics, National Institute of Child Health and Human Development, National Institutes of Health, Bethesda, Maryland.

²National Institute of Neurological Disorders and Stroke, National Institutes of Health, Bethesda, Maryland.

³Computational Bioscience and Engineering Laboratory, Center for Information Technology, National Institutes of Health, Bethesda, Maryland.

Grant sponsor: Intramural Research Program of the National Institute of Child Health and Human Development (NICHD), National Institutes of Health.

*Correspondence to: Michal E. Komlosh, PhD, National Institutes of Health, 13 South Dr., MSC 5772, Bldg. 13, Rm. 3W16, Bethesda, MD 20892-5772. E-mail: komloshm@yahoo.com.

Received 2 July 2007; revised 1 November 2007; accepted 3 December 2007.

DOI 10.1002/mrm.21528

Published online in Wiley InterScience (www.interscience.wiley.com).

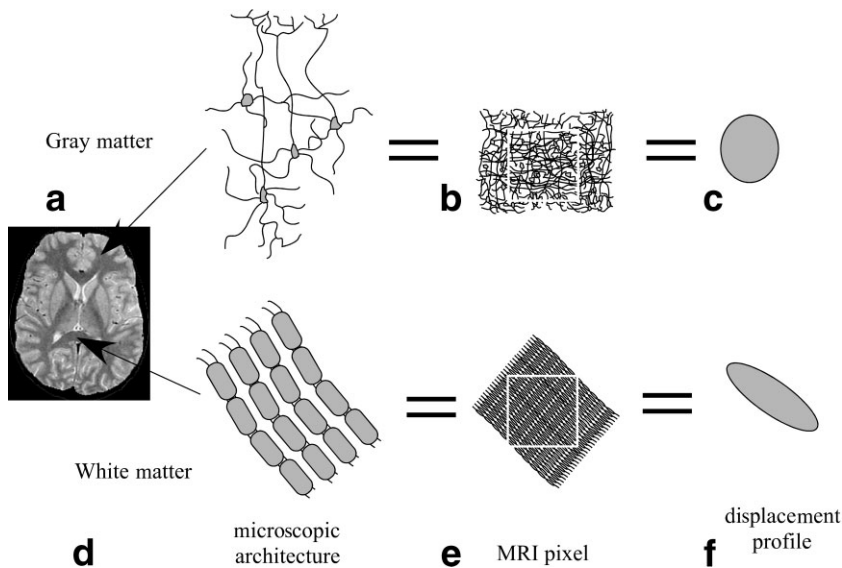


FIG. 1. **a,d**: Illustration of gray and white matter microscopic architecture. **b,e**: Illustration of gray and white matter structure at an MRI pixel length scale. **c,f**: The resulting pixel-averaged diffusion ellipsoids.

a different application—to calculate the size of restricted tissue compartments. This was done by systematically varying the angle between the q-vectors applied in the two PGSE blocks, and fitting the resulting echo attenuation profile to a formula proposed by Mitra (9) that depends explicitly on the pore size. Although cell size can be measured using a d-PGSE sequence, the two PGSE blocks must be applied consecutively, i.e., with no evolution or mixing time between them (9,16).

In this study we implemented d-PGSE MRI by first applying a d-PGSE NMR sequence as a “filter” that was then concatenated to an MRI block (Fig. 2). We first applied this imaging method to confirm that an isotropic liquid phantom was indeed spatially uniform and microscopically isotropic. We then used this sequence to detect anisotropy

in a previously described “gray matter” phantom (15) and evaluated the method by comparing imaging data we obtained to that obtained using d-PGSE NMR spectroscopy. The d-PGSE filtered MRI sequence was then used to obtain d-PGSE weighted MRI (d-DWI) data in fixed pig spinal cord.

MATERIALS AND METHODS

As mentioned above, the d-PGSE MRI sequence used in this study was constructed from a d-PGSE NMR block followed by a gradient echo MRI block. In all d-PGSE experiments the diffusion weighting was varied by keeping the gradient pulse duration constant while stepping up strength simultaneously in both PGSE blocks. The d-PGSE filtered MRI sequence was first tested on an isotropic sample of 5 cSt polydimethylsiloxane (PDMS, Sigma-Aldrich, St. Louis, MO) to ensure system performance and to evaluate the possible disparity between the spectroscopy and imaging echo attenuations. The experiment was performed using nine different gradient combinations, three collinear (X_X, Y_Y, Z_Z) and six orthogonal ($X_Y, Y_X, X_Z, Z_X, Y_Z, Z_Y$). The set of diffusion parameters used for the d-PGSE blocks are: diffusion gradient pulse duration (δ) = 3 ms, diffusion time (Δ) = 40 ms, and mixing time (τ_m) = 15 ms. Sixteen values of gradients were used in the spectroscopy experiment with the strength (G) varied between 0 and 250 mTm^{-1} . Five gradient values were used in the imaging experiment, (G) = 0, 44.3, 73.8, 147.6, 221.4 mTm^{-1} . The parameters used for the imaging block were: matrix size = 128×64 , field of view (FOV) = $7 \times 7 \text{ mm}^2$, slice thickness = 4 mm, echo time/repetition time (TE/TR) = 6 ms / 4 sec, and acquisition time per direction of 8.5 min; signal-to-noise ratio (S/N) ≈ 200 . For measuring the echo attenuation intensities a region of interest (ROI) (Fig. 3) was taken within the center of the phantom to avoid artifacts originating from Gibbs ringing (17).

A previously described “gray matter” phantom (15) was used as a microscopically anisotropic, macroscopically isotropic construct. It consists of 0.5-mm-long fused silica

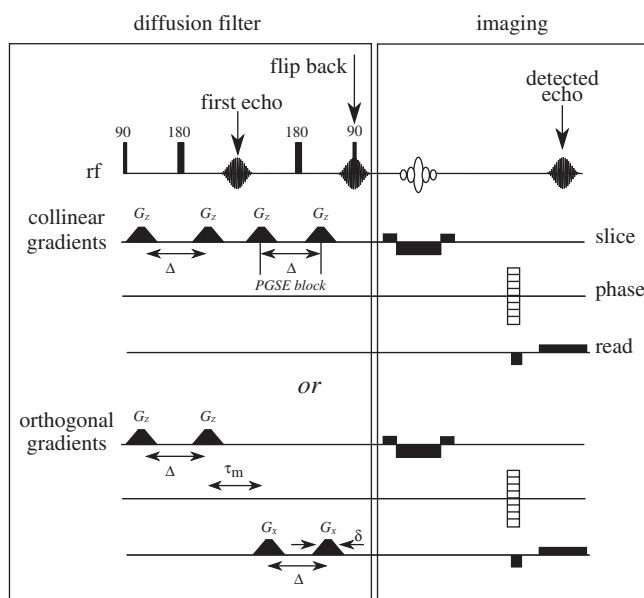


FIG. 2. d-PGSE filtered MRI pulse sequence. τ_m , the mixing time, is the time between the two d-PGSE blocks.

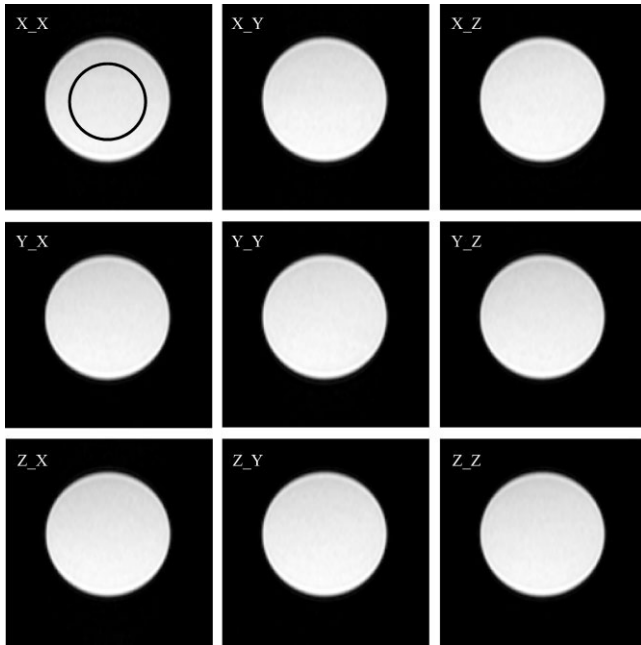


FIG. 3. d-PGSE filtered MRI of PDMS obtained for the nine collinear and orthogonal gradient combinations using a gradient strength of 73.8 mT m^{-1} . The ROI used in the analysis is marked.

glass tubes with ID = $20 \mu\text{m}$ and OD = $90 \mu\text{m}$ (Polymicro Technologies, Phoenix, AZ) filled with water and randomly immersed in deuterated 1,2-dichlorobenzene (Cambridge Isotope Laboratories, Andover, MA). The tubes were filled with water by condensation of water vapor on the inner walls of the tubes.

The d-PGSE filtered MRI sequence was used to image this phantom in the same nine different gradient combinations as the isotropic PDMS phantom described above. Although in theory d-PGSE data obtained with one collinear and one orthogonal direction are sufficient to detect microscopic anisotropy of the phantom, the application of all nine direction combinations provides an additional control for scanner performance. The imaging data were again compared to data acquired by the spectroscopic sequence of d-PGSE.

The set of diffusion parameters used for the d-PGSE blocks were: $\delta = 3 \text{ ms}$, $\Delta = 40 \text{ ms}$, and $\tau_m = 35 \text{ ms}$. Twenty-one values of gradients were used in the spectroscopy experiment, the strength (G) varied between 0 and 241 mTm^{-1} . Four gradient values were used in the imaging experiment: (G) = 0, 73.8, 147.6, 221.4 mTm^{-1} . The parameters used for the imaging block were: matrix size = 32×32 , FOV = $10 \times 10 \text{ mm}^2$, slice thickness = 4 mm, TE/TR = 2.7 ms / 7 sec, and acquisition time per direction of 15 min. In order to compare the echo attenuation intensities of the imaging experiment to the spectroscopy experiment (which measures the entire volume within the RF coil) adequately, an ROI, which covers the entire image (ROI-1 in Fig. 5) excluding its edge to avoid artifacts originating from Gibbs ringing, was chosen. Two additional ROIs (ROI-2 and ROI-3) were chosen from different regions within the phantom. The S/N of this experiment: ROI-1 ≈ 30 , ROI-2 ≈ 40 ROI-3 ≈ 23 .

A formalin-fixed pig spinal cord obtained from necropsy was rehydrated and immersed in perfluoropolyether (Fomblin, LC/8, Solvay Solexis, Brussels, Belgium) to minimize susceptibility differences between the tissue and its surrounding. Fomblin is immiscible in water and does not produce a proton signal. The sample was placed in a 10mm NMR tube (Shigemi, Japan), and then capped with a plunger. The long axis of the cord was oriented along the tube's Z-axis. The susceptibility of both the tube and plunger matches that of D_2O . This specimen fixture design ensures minimal susceptibility differences between the specimen and container, while minimizing sample motion during scanning. The d-PGSE MRI experiment was performed by applying three collinear gradient combinations: X_X, Y_Y, and Z_Z, and two orthogonal ones: X_Y and Y_X. The set of diffusion parameters used for the d-PGSE blocks are: diffusion parameters: $\delta = 3 \text{ ms}$, $\Delta = 15 \text{ ms}$, $\tau_m = 75 \text{ ms}$. The experiment was performed using two gradient strengths, 0 and 340 mTm^{-1} . The parameters used for the imaging block were: matrix size = 128×128 , FOV = $12 \times 12 \text{ mm}^2$, slice thickness = 1 mm, TE/TR = 3.11 ms/4 sec, acquisition time per direction was 136 min. Six ROI were chosen following (18): left lateral (LLW), right lateral (RLW), dorsal (DW), and ventral (VW) white matter, and right (RG) and left (LG) gray matter. The S/N of this experiment: LLW ≈ 21 , RLW ≈ 22 , VW ≈ 26 , DW ≈ 18 , LG ≈ 27 , RG ≈ 27 .

All experiments were performed at a temperature of $20.8 \pm 0.1^\circ\text{C}$ on a 7T vertical bore Bruker Avance MR imaging system equipped with a Micro2.5 microimaging probe, having a maximum gradient strength of $24.65 \text{ mTm}^{-1}\text{Amp}^{-1}$ in three orthogonal directions with a nominal peak gradient current supply of 60 Amp per channel. The number of scans varied depending on sample sensitivity.

RESULTS

Figure 3 shows d-PGSE-weighted MRI of PDMS acquired with a diffusion gradient strength of $G = 73.8 \text{ mTm}^{-1}$. Collinear and orthogonal d-PGSE-weighted MRI are shown to illustrate that in a microscopically isotropic specimen, there are no differences observed between these two images. No visible imaging artifacts are observed, such as susceptibility, eddy currents, RF inhomogeneity, etc.

Figure 4 shows the echo attenuations versus b-value [$\gamma^2 G^2 \delta^2 (\Delta - \delta/3)$] for d-PGSE filtered MRI (filled symbols) and d-PGSE NMR spectroscopy (open symbols) for the isotropic PDMS sample. Echo attenuations using all nine combinations of gradient directions coalesce, which indicates that there are no observable acquisition-related artifacts. Furthermore, attenuation profiles for d-PGSE spectroscopy and imaging are also very close, which demonstrates that adding the imaging block has a minimal effect on the echo signal.

Figure 5 shows an image of the “gray matter” phantom acquired with the d-PGSE filtered MRI sequence with $G = 59 \text{ mTm}^{-1}$. The intensity variation across the image is most likely due to differences in the packing density of tubes caused by aggregation and nonuniform sedimentation during the process of making the phantom. Neverthe-

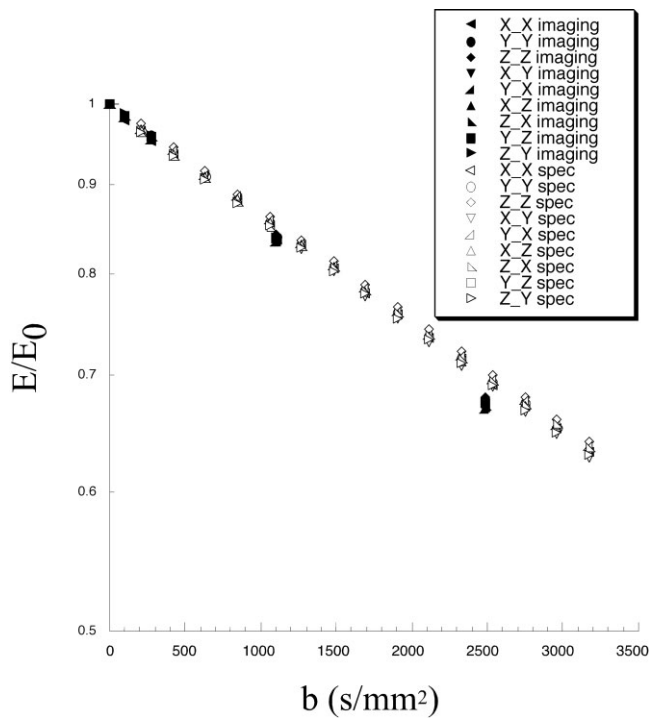


FIG. 4. Echo attenuation versus b -value for d-PGSE filtered MRI (filled symbols) and NMR spectroscopy (open symbols) in PDMS with $\delta = 3$ ms, $\Delta = 40$ ms, $\tau_m = 15$ ms, $G_{\max} = 440$ mT m $^{-1}$, matrix size = 128×64 , FOV = 7×7 mm 2 , slice thickness = 4 mm, TE/TR = 6 ms / 4 sec.

less, artifacts resulting from the MR scanner are not observed.

Figure 6 shows the echo attenuation from d-PGSE versus b -value for MRI (filled symbols) and NMR spectroscopy (open symbols) in the “gray matter” phantom. The echo attenuations resulting from the orthogonal PGSE block combinations drop more rapidly with respect to b -value than the echo attenuations resulting from the collinear PGSE block combinations. This clearly indicates microscopic anisotropy. Experimental curves for the d-PGSE MR imaging and spectroscopy coalesce, which further supports the findings that the addition of the imaging block does not affect our localized d-PGSE spectroscopic measurements. Note, the attenuation resulting from the Z_Z gradient direction appears less than that of the other collinear directions. This difference might be due to nonuniform sedimentation of the tubes during the preparation of the phantom. It seems that there is a slight preference for tube settling in the perpendicular direction to the NMR tube axis. This would result in somewhat more restriction in the Z direction.

To examine the nonuniform tube sedimentation two additional ROIs (ROI 2 and 3) shown in Fig. 5 were chosen. Figure 7 shows the echo attenuation versus b -values for ROI-2 (Fig. 7a) and ROI-3 (Fig. 7b), respectively, compared with the spectroscopy results shown in Fig. 6. All the echo attenuations resulting from the collinear gradient direction combination in ROI-2 superimpose, which implies random tubes orientation in this part of the phantom, while ROI-3 shows additional restriction along the z-axis. The

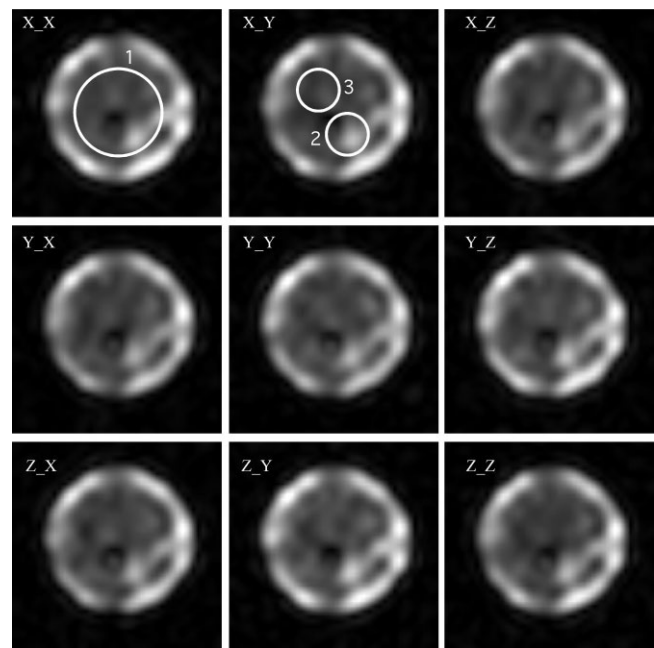


FIG. 5. d-PGSE filtered MRI in a “gray matter” phantom for the nine collinear and orthogonal gradient combinations using a gradient strength of 59 mT m $^{-1}$. The three ROIs used in the analysis are marked.

spectroscopy echo attenuation appears to be the average of signal from these two ROIs given that the signal is acquired from the entire sample and the heterogeneous nature of the phantom cannot be observed. The signal from the orthog-

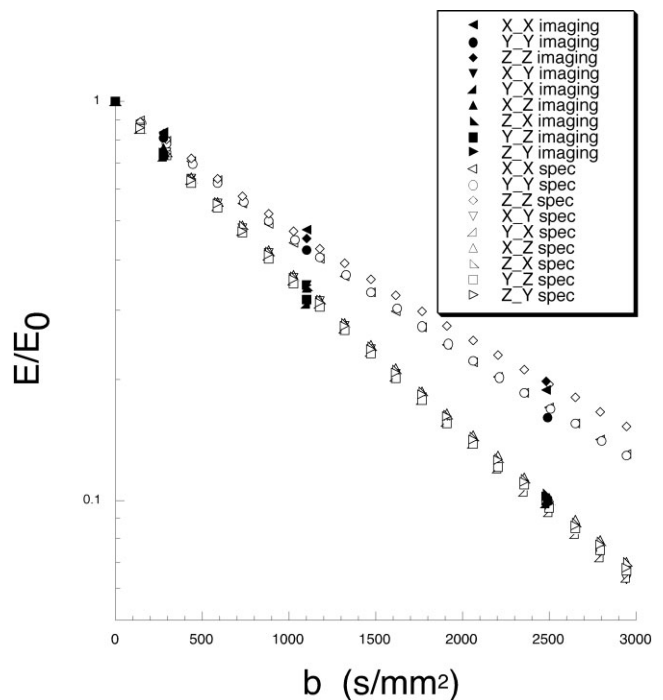


FIG. 6. d-PGSE filtered MR echo attenuation of ROI-1 versus b -value in the “gray matter” phantom using MRI (filled symbols) and NMR spectroscopy (open symbols). $\delta = 3$ ms, $\Delta = 40$ ms, $\tau_m = 35$ ms, $G_{\max} = 221$ mT m $^{-1}$, matrix size = 32×32 , FOV = 10×10 mm 2 , slice thickness = 4 mm, TE/TR = 2.7 ms / 7 sec.

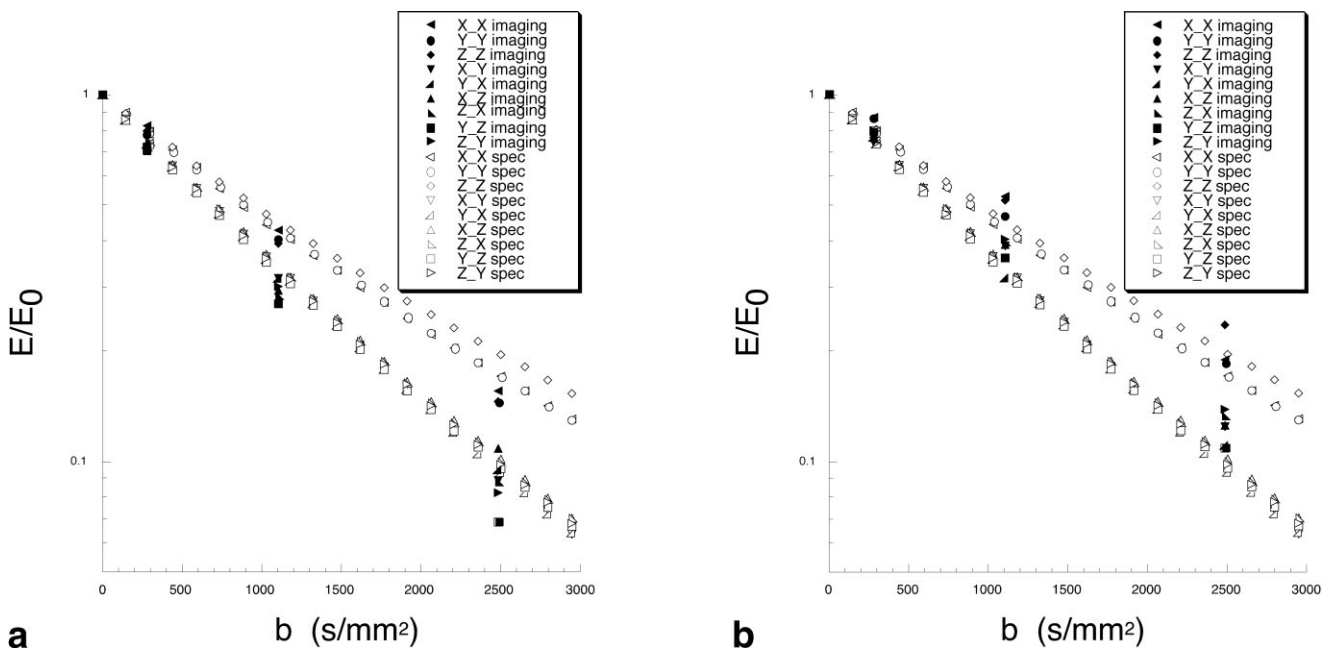


FIG. 7. d-PGSE filtered MR echo attenuation of (a) ROI-2 and (b) ROI-3 versus b-value in the “gray matter” phantom using MRI (filled symbols) and NMR spectroscopy (open symbols). $\delta = 3$ ms, $\Delta = 40$ ms, $\tau_m = 35$ ms $G_{max} = 221$ mT m⁻¹, matrix size = 32 × 32, FOV = 10 × 10 mm², slice thickness = 4 mm, TE/TR = 2.7 ms / 7 sec.

onal direction combination is also affected by the slight macroscopic anisotropy and in ROI-3 the attenuation is less than in ROI-2. Nevertheless, even though slight macroscopic anisotropy can be observed in different regions of the phantom, the difference between the orthogonal and collinear echo attenuation is due to the microscopic anisotropy, as can be observed in the region of the phantom where the tubes are completely random, such as in ROI-2.

Figure 8 presents the difference between the average collinear signal, $\left(\frac{E_{X_X}}{E_0} + \frac{E_{Y_Y}}{E_0} + \frac{E_{Z_Z}}{E_0}\right) / 3$, and the average orthogonal signal, $\left(\frac{E_{X_Y}}{E_0} + \frac{E_{Y_X}}{E_0} + \frac{E_{X_Z}}{E_0} + \frac{E_{Z_X}}{E_0} + \frac{E_{Y_Z}}{E_0} + \frac{E_{Z_Y}}{E_0}\right) / 6$, echo attenuation values versus b-value. Both imaging and spectroscopy data are similar. The magnitude of the difference between the collinear and orthogonal curves depends on the b-value, increasing to a maximum at a gradient of 148 mTm⁻¹ and then decreasing.

Figure 9a shows a non-d-PGSE-weighted MRI (i.e., with $G = 0$) containing gray and white matter ROIs. Figure 9b shows the ROI-averaged echo attenuation profiles. As expected, the echo attenuation profiles for the X_X and Y_Y directions in both gray and white matter are similar, while the attenuation profiles in the Z_Z direction are significantly greater, which indicates macroscopic anisotropy in the spinal cord. The echo attenuation for the Z_Z direction, however, is greater for white matter than for gray matter, suggesting greater macroscopic diffusion anisotropy in white matter than gray matter, consistent with DTI findings. The echo attenuation of the X_Y and Y_X orthogonal gradient combinations is greater than along the collinear directions of X_X and Y_Y, indicating an additional microscopic anisotropy in the plane perpendicular to the principal axis of the spinal cord.

DISCUSSION

While we chose here to use a d-PGSE NMR block followed by a gradient echo MRI block, any combination of double-pulsed gradient NMR and MRI blocks could be used. For instance, for a specimen having a short T_2 it would be prudent to substitute the d-PGSE NMR block with a stim-

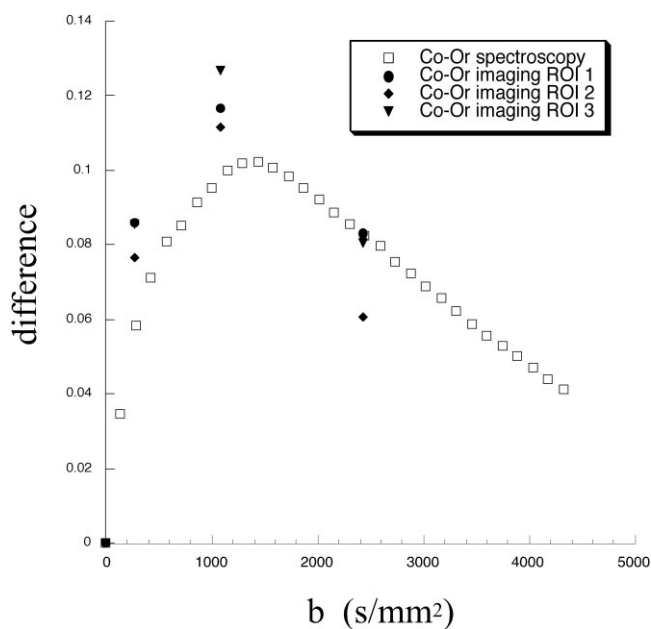


FIG. 8. Difference between the collinear and orthogonal echo attenuation versus b-value profiles for d-PGSE MRI (filled symbols) and NMR spectroscopy (open symbols) in the “gray matter” phantom.

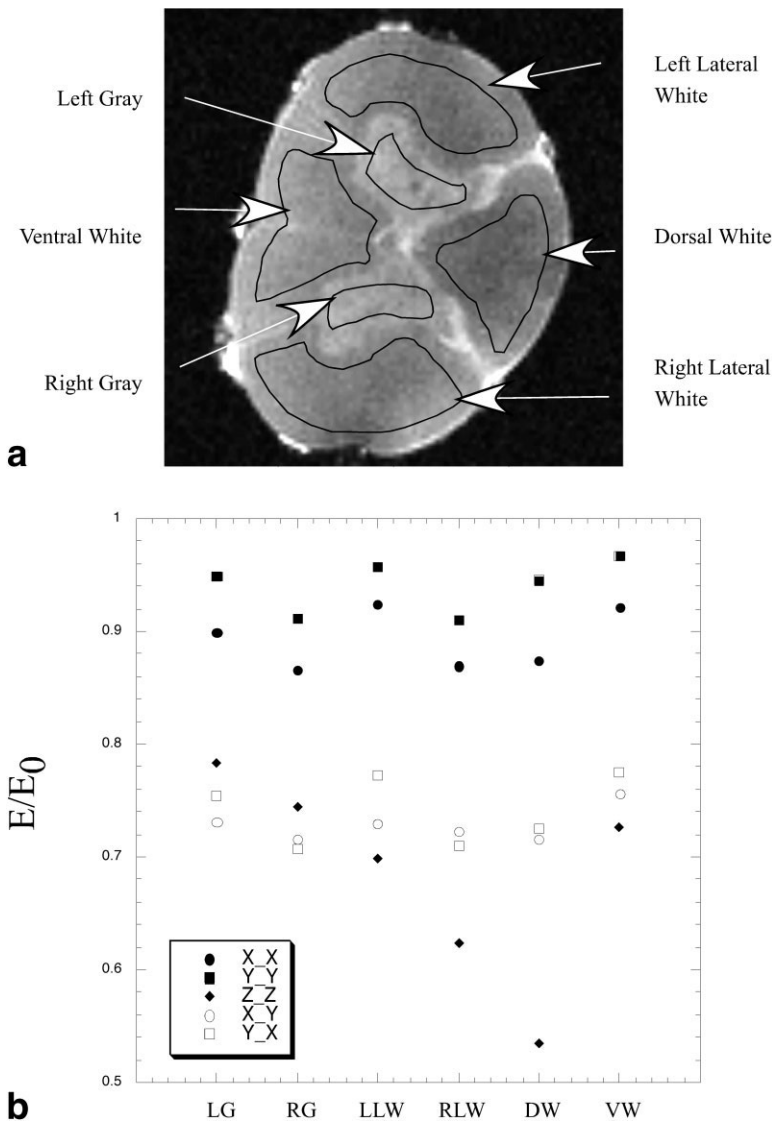


FIG. 9. **a:** d-PGSE filtered MRI of pig spinal cord for $b = 0$ with the gray and white matter regions of interest (ROIs) marked. **b:** Echo attenuation for the collinear and orthogonal direction using pixels from the marked ROIs.

ulated echo variant, like the one used by Cheng and Cory (10) and Khrapichev and Callaghan (19). We chose to use the d-PGSE NMR sequence as a filter, rather than incorporating it within the MR imaging block itself, despite the fact that the latter arrangement has better S/N characteristics, to avoid: 1) artifacts resulting from RF inhomogeneity when using shaped pulses, and 2) cross-terms that invariably arise between the imaging and diffusion gradients, particularly in micro-imaging applications.

The similarity of our spectroscopy and imaging results in Figs. 4 and 6 clearly demonstrates that the d-PGSE filtered MRI sequence does not alter the resulting echo attenuation profiles one would obtain using d-PGSE NMR spectroscopy.

Figures 6 and 7 demonstrate the presence of microscopic anisotropy in the “gray matter” phantom. The difference in echo attenuations between the two families of curves, orthogonal versus collinear, indicates microscopic anisotropy and is a signature of local anisotropy. Although the phantom theoretically supposed to be homogenous in nature consists of only one type of tubes, in practice the sedimentation process was not uniform.

The difference curve obtained using the “gray matter” phantom presented in Fig. 8 shows that although microscopic anisotropy can be detected in the low b -value regime, there is a clear region where this anisotropy is most visible. Acquisition of the entire curve using numerous gradient strength pulses as demonstrated in the spectroscopy data in Fig. 6 can potentially provide information about the nature of the anisotropy and the architecture of the sample and may eventually be fit to a suitable model (9–11,15). However, this imaging experiment is time-consuming, which limits the number of b -values that can be used when the study involves fresh tissue, in situ, and in vivo specimens. In order to achieve sufficient spatial resolution while keeping the experiment time short, only one b -value greater than zero can be used currently. Performing the experiment using only one optimal b -value where the anisotropy is most visible could reduce experimental time for MRI applications using this new contrast mechanism. Alternatively, teaming the d-PGSE filter with a fast imaging method might enable the use of multiple b -values for each gradient direction combination.

Indeed, owing to the low S/N of the fixed sample and the high resolution needed to observe fine structures, d-PGSE MRI experiments on the pig spine, shown in Fig. 8, were performed using only one b-value that was chosen after preliminary experiments were performed. Differences among the intensities arising from different collinear gradient combinations observed in the spinal cord are an indicator of macroscopic anisotropy. The echo attenuation along the longitudinal axis of the spinal cord is greater than along its two perpendicular axes. As expected, due to the numerous collateral nerves (20) oriented perpendicular to the longitudinal axis of the spine, macroscopic anisotropy in the gray matter is somewhat lower than in white matter (21,22). The echo attenuations resulting from the orthogonal gradient direction combinations in both white and gray matter are greater than those resulting from the collinear gradient combination, indicating that microscopic anisotropy is present in the XY plane. This anisotropy is generally not apparent using conventional DWI techniques, such as DTI, which measures similar diffusion coefficients along those directions. However, comparing collinear and orthogonal gradient combinations using the d-PGSE reveals microscopic anisotropy. This anisotropy could originate in fibers, which are randomly oriented in that plane such as the collateral nerve fibers that are skewed.

CONCLUSION

A novel d-PGSE MRI sequence was presented to provide new information about tissue microstructure. Specifically, it can be used to detect microscopic diffusion anisotropy even in macroscopically isotropic specimen. The addition of an imaging block to a d-PGSE NMR sequence has a small effect on the echo attenuation and does not appear to change the ability to detect this anisotropy. The method was tested on polymer and tissue phantoms, as well as in fixed pig spinal cord, where both macroscopic anisotropy and microscopic anisotropy were detected in gray and white matter. Microscopic anisotropy was also detected in the low b-value regime, in a range accessible to many clinical and small animal scanners. This finding suggests that multiple-pulsed gradient MRI could provide a new source of image contrast in biological research applications and possibly in clinical studies.

ACKNOWLEDGMENTS

The authors thank Dr. H.D. Morris for helping with all technical aspects of the experiments, and Dr. R.E. Rycyna from Bruker Biospin for writing the initial d-PGSE imaging sequences. We also thank those who were involved in providing this research with the pig spinal cord tissue: Mr. R.R. Clevenger, Mr. T.J. Hunt, Ms. G.J. Zywicke, Mr. A.D. Zetts, Mrs. K. Keeran, Mr. S.M. Kozlov, and Mr. K.R. Jeffries, from LAMS, NHLBI. We thank Liz Salak for editing the article.

REFERENCES

1. Basser PJ, Mattiello J, LeBihan D. MR diffusion tensor spectroscopy and imaging. *Biophys J* 1994;66:259–267.
2. LeBihan D, Breton E, Lallemand D, Grenier P, Cabanis E, Laval-Jeantet M. MR imaging of intravoxel incoherent motion: application to diffusion and perfusion in neurologic disorders. *Radiology* 1986;161:401–407.
3. Moseley ME, Cohen Y, Kucharczyk J, Mintorovich J, Asgari HS, Wendland MF, Tsuruda J, Norman D. Diffusion-weighted MR imaging of anisotropic cat central nervous system. *Radiology* 1990;176:439–445.
4. Pierpaoli C, Jezzard P, Basser PJ, Barnett A, Di Chiro G. Diffusion tensor MR imaging of the human brain. *Radiology* 1996;201:637–648.
5. Ronen I, Kim K-H, Garwood M, Ugurbil K, Kim D-S. Conventional DTI vs. slow and fast diffusion tensor in cat visual cortex. *Magn Reson Med* 2003;49:785–790.
6. Ma X, Kadah YM, LaConte SM, Hu X. Enhancing measured diffusion anisotropy in gray matter by eliminating CSF contamination with FLAIR. *Magn Reson Med* 2004;51:423–427.
7. Bhagat YA, Beaulieu C. Diffusion anisotropy in subcortical white matter and cortical gray matter: changes with aging and the role of CSF — suppression. *J Magn Reson Imaging* 2004;20:216–227.
8. Stejskal EO, Tanner JE. Spin diffusion measurement: spin echo in the presence of time-dependent field gradient. *J Chem Phys* 1965;42:288–292.
9. Mitra PP. Multiple wave-vector extension of the NMR pulsed-field-gradient spin-echo diffusion measurement. *Phys Rev B* 1995;51:15074–15078.
10. Cheng Y, Cory DG. Multiple scattering by NMR. *J Am Chem Soc* 1999;121:7935–7936.
11. Callaghan PT, Komlosh ME. Locally anisotropic motion in a macroscopically isotropic system: displacement correlation measured using double pulsed gradient spin-echo NMR. *Magn Reson Chem* 2002;40: S15–S19.
12. Callaghan PT, Furo I. Diffusion-diffusion correlation and exchange as a signature for local order and dynamics. *J Chem Phys* 2004;120:4032–4038.
13. Callaghan PT, Godfroy S, Ryland BN. Use of the second dimension in PGSE NMR studies of porous media. *Magn Reson imaging* 2003;21: 243–248.
14. Qiao Y, Galvosas P, Callaghan PT. Diffusion correlation NMR spectroscopic study of anisotropic diffusion of water in plant tissue. *Biophys J* 2005;89:2899–2905.
15. Komlosh ME, Horkay F, Freidlin RZ, Nevo U, Assaf Y, Basser PJ. Detection of microscopic anisotropy in gray matter and in novel tissue phantom using double pulsed gradient spin echo MR. *J Magn Reson* 2007;189:38–45.
16. Koch MA, Finsterbusch J. Multiple wave vector diffusion experiments on restricted diffusion. In: *Proc 13th Annual Meeting ISMRM*, Miami Beach, FL; 2005:840.
17. Haacke EM, Brown RW, Thompson MR, Venkatesan R. *Magnetic resonance imaging: physical principles and sequence design*. New York: John Wiley & Sons; 1999.
18. Pattany PM, Puckett WR, Klose KJ, Quencer RM, Bunge RP, Kasuboski L, Weaver RG. High-resolution diffusion-weighted MR of fresh and fixed cat spinal cord: evaluation of diffusion coefficients and anisotropy. *Am J Neuroradiol* 1997;18:1049–1056.
19. Khrapichev AA, Callaghan PT. Double PGSE NMR with stimulated echoes: phase cycles for the selection of desired encoding. *J Magn Reson* 2001;152:259–268.
20. Cajal SR. *Histology of the nervous system of man and vertebrates*. Swanson N, Swanson LW, translators. New York: Oxford University Press; 1995.
21. Holder CA, Muthupillai R, Mukundan S, Eastwood JD, Hudgin PA. Diffusion-weighted MR imaging of the normal human spinal cord in vivo. *Am J Neuroradiol* 2000;21:1799–1806.
22. Mamata H, Girolami UD, Hoge WS, Jolesz FA, Maier SE. Collateral nerve fibers in human spinal cord: visualization with magnetic resonance diffusion tensor imaging. *Neuroimage* 2006;31:24–30.